Biosensors and Bioelectronics 83 (2016) 142–148

Contents lists available at ScienceDirect

Biosensors and Bioelectronics

journal homepage: www.elsevier.com/locate/bios

Increased electrocatalyzed performance through hairpin oligonucleotide aptamer-functionalized gold nanorods labels and graphene-streptavidin nanomatrix: Highly selective and sensitive electrochemical biosensor of carcinoembryonic antigen

Wei Wen [a,b], Jing-Yi Huang [b], Ting Bao [b], Jun Zhou [c], Hong-Xing Xia [a], Xiu-Hua Zhang [b], Sheng-Fu Wang [b,*], Yuan-Di Zhao [a,*]

[a] Britton Chance Center for Biomedical Photonics at Wuhan National Laboratory for Optoelectronics–Hubei Bioinformatics & Molecular Imaging Key Laboratory, Department of Biomedical Engineering, College of Life Science and Technology, Huazhong University of Science and Technology, Wuhan 430074, PR China

[b] Hubei Collaborative Innovation Center for Advanced Organic Chemical Materials, Ministry of Education Key Laboratory for the Synthesis and Application of Organic Functional Molecules & College of Chemistry and Chemical Engineering, Hubei University, Wuhan 430062, PR China

[c] Department of Clinical Laboratory, Wuhan Commercial Staff Hospital, Wuhan 430021, PR China

ARTICLE INFO

Article history:
Received 29 February 2016
Received in revised form
8 April 2016
Accepted 14 April 2016
Available online 14 April 2016

Keywords:
Hairpin oligonucleotide-functionalized gold nanorods
Horseradish peroxidase
Graphene-streptavidin nanomatrix
Electrochemical biosensor
Carcinoembryonic antigen

ABSTRACT

We report a triplex signal amplification strategy for sensitive biosensing of cancer biomarker by taking advantage of hairpin-shaped oligonucleotide-functionalized gold nanorods (HO-GNRs), graphene and the avidin-biotin reation. The strategy expands electrochemical detection of carcinoembryonic antigen (CEA) by using an aptamer as biosensor's recognition element and HO-GNRs as signal enhancer. To construct this biosensor, the GNR was used as a carrier of horseradish peroxidase (HRP) and HO aptamer with a biotin at the 3′-end and a thiol at the 5′-end, which amplified the electrochemical response because of a large molar ratio of HRP to HO. In the presence of target CEA, the binding reactions of CEA with the loop portions of the HOs caused HOs' loop-stem structure opened and exposed the biotins, and then HRP-GNRs-HO conjugates were captured on graphene and streptavidin modified electrodes via the reaction between the exposed biotins and preimmobilized streptavidins. The accumulation of HRP effectively catalyzed the hydrogen peroxide-mediated oxidation of *o*-phenylenediamine to generate an electrochemical reduction current for CEA detection. Under optimal conditions, the electrochemical biosensor exhibited a wide dynamic range of 5 pg mL^{-1} and 50 ng mL^{-1} toward CEA standards with a low detection limit of 1.5 pg mL^{-1} (signal-to-noise ratio of 3). The proposed biosensor accurately detected CEA concentration in 8 human serum samples from patients with lung diseases, showing excellent correlations with standard chemiluminescence immunoassay. Furthermore, these results of target DNA detection made it abundantly clear that the proposed strategy can also be extended for detection of other relative biomarkers using different functional DNA structures, which shows great prospects in single-nucleotide polymorphisms analysis, biomedical sensing and application for accurate clinical diseases diagnostic.

1. Introduction

Ultrasensitive and highly selective determination of disease-specific protein biomarkers has important significance in many aspects of elaborating the pathogenic mechanism of disease and elucidating the rule of pathological changes, early diagnosis and therapy of disease, development and screening of new drug, etc (Ge et al., 2016). Carcinoembryonic antigen (CEA), as a broad-spectrum tumor marker, is elevated in many malignancies, such as gastric cancer, colorectal cancer, breast cancer, liver cancer and pancreatic cancer. Significant CEA positivity has been reported for reflecting disease progression or regression status, and its levels be identified in monitoring responses to treatment and the early diagnosis of recurrences. Much attention has been focused on the detection of low-abundance CEA using an electrochemical (Zhou et al., 2013; Xue et al., 2015), electrochemiluminescent (Deng et al., 2013), surface-enhanced Raman scattering (Chon et al., 2009),

* Corresponding authors.
E-mail addresses: wangsf@hubu.edu.cn (S.-F. Wang), zydi@mail.hust.edu.cn (Y.-D. Zhao).

http://dx.doi.org/10.1016/j.bios.2016.04.039
0956-5663/

fluorescent (Wang et al., 2014), mass spectrometric (Liu et al., 2011), chemiluminescent (Zong et al., 2012; Wang et al., 2015), or surface plasmon resonance (Springer et al., 2013) techniques. Nevertheless, most of these biosensors use antibody as molecular recognition element and suffer from some intrinsic drawbacks: expensive consumption because of having to use cell lines or animals to produce, poor stability limiting transport and application in harsh conditions (e.g., high temperature or extreme pH), and high molecular weight impeding its ability to penetrate into the deep site of the biosensor, et al. It is very important to explore novel molecular recognition tools for the development of protein biomarkers determination with more promising performances such as low cost, high stability and simplicity. An aptamer is a short, chemically synthesized, single-stranded DNA/RNA oligonucleotide that can fold into a unique secondary or tertiary structures structure that recognizes a specific targets ranging from small molecules to even proteins or cells (Lao et al., 2015). Compared to antibodies, aptamer holds several unique advantages as non-immunogenicity, easier to mass reproducible synthesis, rapid tissue penetration, easy functionalization, faster blood plasma clearance and high stability (Iliuk et al., 2011; Pu et al., 2015). However, there are only few reports on aptamer against CEA protein. In 2010, Tabar and Smith (Tabar and Smith, 2010) firstly selected DNA aptamers against CEA for clinically imaging and diagnosis of cancer cells. Later, Chen and his group developed aptamer-based CEA determination using fluorescent (Lin et al., 2012) and colorimetric (Liang et al., 2014) biosensor. Unfortunately, exploration of the DNA aptamer as electrochemical biosensor's recognition element for CEA determination is still sparse (Shu et al., 2013; Xue et al., 2015). Coupling of the significant advantages of aptamers with high sensitivity, robustness, fast response and the potential for minituarization of electrochemical methods, we postulated that electrochemical detection of CEA in aptasensor may offer a prospective approach for highly sensitive and selective determination of disease-specific protein biomarkers.

Hairpin-shaped oligonucleotides (HO), also called molecular aptamer beacons, consist of a base-paired stem structure and a loop sequence of aptamer with unpaired nucleotides, which holds the advantages of both the generality of an aptamer and the good signal switching capability of molecular beacon (Huang et al., 2014). Besides the merits of linear aptamers, HO also have inherent a target-induced conformation change mechanism that enables the determination of targets without the separation of unbound probes. Furthermore, the thermodynamic stability of the unique stem-loop structure makes HO exceptional linear aptamers with excellent selectivity, which involve HO widely used in biosensor development to achieve low background and high accuracy (Wang et al., 2009). The sensitivities of HO based biosensors have been improved by the combinations of HO with graphene oxide (He et al., 2011), DNAzymes (Zuo et al., 2010), or the modifications of HO with gold nanoparticles (He et al., 2010; Fan et al., 2011), quantum dots (Kim et al., 2004; Zhang et al., 2015). Among different kinds of signal enhancers, gold nanorods (GNRs), which possess distinctive chemical and physical properties as a typical elongated gold nanostructure, have rapidly become powerful base platforms for biosensing, bioimaging and nanomedical applications (Chen et al., 2013). Compared with similarly sized spherical nanoparticles, GNRs exhibit higher absorption, both transverse and longitudinal localized surface plasmon resonances, inherently more sensitive to the local dielectric environment and can convert light into heat through various nonradiative photophysical processes. In addition, GNRs can be easily functionalized via simple thiolate chemistry. However, according to our knowledge, few attentions have been paid to the employment of HO-functionalized GNRs probes for highly selective and sensitive detection of protein biomarkers in an electrochemical biosensing system.

Herein, a new triplex signal amplification electrochemical biosensor by taking advantage of the HO-functionalized GNRs probes, graphene and the avidin-biotin reation was reported for CEA detection. As shown in Scheme 1, the HO-functionalized GNRs probes were prepared by a self-assembling process of a hairpin oligonucleotide modified with a biotin at the 3′-end and a thiol at the 5′-end on the surface of GNR. Then horseradish peroxidase (HRP) was also conjugated to the surface of GNR to prepare HRP-GNRs-HO conjugate, and could easily use as an electrochemical tracing label. Graphene (GR), which presents excellent electron-transfer ability, large surface area, favorable biocompatibility and so on (Xu et al., 2015; Tang et al., 2015), was employed to increase the effective surface area for the loading of streptavidin (SA) on the surface of electrode and accelerate the electron transfer of electroactive species. In the presence of CEA, the binding reactions of target CEA with the loop portions of the HOs on the GNRs surface opened the stem of the HOs and exposed the biotins which were located at the end of HOs. Then the HRP-GNRs-HO conjugates associated with the activated biotins were captured on GR and streptavidin modified electrodes via the reaction between the exposed biotins and preimmobilized streptavidins. The captured HRP effectively catalyzed the hydrogen peroxide-mediated oxidation of *o*-phenylenediamine (oPD) in solution, and an enzymatic generation of 2, 3-diaminophenazine (DAP) was produced as redox probe (Hamilton et al., 1999; Cui et al., 2008), enabling electrochemical detection of CEA. In the absence of CEA, The HO on the GNR surface maintained its hairpin structure, and the biotin groups stayed 'inactive', and the HRP-GNRs-HO conjugates were not captured on the sensor electrode, resulting a very limited background current. The as-proposed triple signal amplification electrochemical biosensor shows great promise in clinical diagnostics for detection of cancer biomarkers, and it is fairly easy to generalize this approach to detect target DNA.

2. Experimental sections

2.1. Reagents

Carcinoembryonic antigen (CEA, from human fluids), tris(2-carboxyethyl)phosphine (TCEP), $NaBH_4$, Cetyltrimetylammonium bromide (CTAB) and streptavidin (SA) were purchased from Sigma-Aldrich. GR was purchased from Sinocarbon Materials Technology Co., Ltd (China). Hydrogen tetrachloroaurate ($HAuCl_4$) was purchased from Alfa Aesar. O-phenylenediamine (oPD) was obtained from Guangcheng Chemical Reagent Co., Ltd (China). Sodium dodecyl sulfate(SDS), $AgNO_3$, horseradish peroxidase (HRP), bovine serum albumin (BSA) were purchased from Sinopharm Chemical Reagent Co., Ltd (China). Deoxyadenosine triphosphate (dATP) and chitosan (CS) were purchased from Aladdin Chemistry Co., Ltd. (China). Clinical serum samples of CEA with different concentrations were provided by the Wuhan Commercial Staff Hospital. All DNA sequences were synthesized and purified by Shanghai Sangon Biotechnology Co., Ltd (Shanghai, China), and their sequences in detail were as follows:

CEA aptamer: 5′-HS-$(CH_2)_6$-CCAC GATA CCAG CTTA TTCA ATTC GTGG-Biotin-3′.

Biotinylated hairpin DNA probe: 5′-HS-$(CH_2)_6$-ACAC GGCA GTTG ATCC TTTG GATA CCCT GGCG TGT-Biotin-3′.

Target DNA: 5′-CCAG GGTA TCCA AAGG ATCA ACTG C-3′.

One base-mismatched DNA: 5′-CCAG GGTA TCCA A**C**GG ATCA ACTG C-3′.

Three base-mismatched DNA: 5′-CCAG GGTA T**GC**G A**C**GG ATCA ACTG C-3′.

DNA oligonucleotide stock solutions were prepared with Tris–HCl buffer (20 mM Tris–HCl, 100 mM NaCl, 5 mM $MgCl_2$, pH = 7.4)

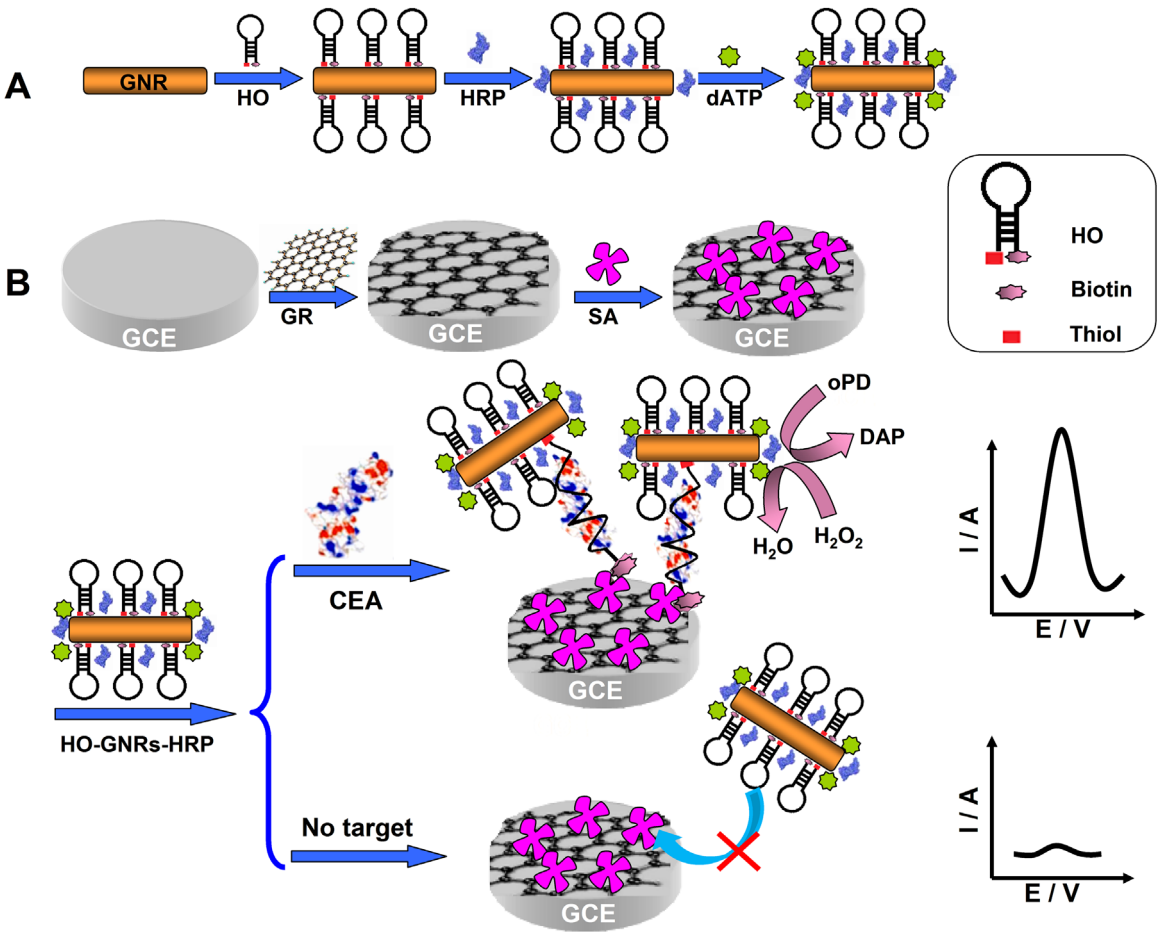

Scheme 1. (A) Modification procedure of HO-GNRs-HRP conjugate. (B) Schematic illustration of the assembly process of SA-CS/GR/GCE and electrochemical sensing strategy for the detection of CEA.

and stored at 4 °C. CEA solutions were prepared with 0.01 M pH 7.4 phosphate buffer solution (PBS). All other chemicals were of analytical reagent grade and used as received. All solutions were prepared with deionized water (18.25 MΩ cm^{-1}) by Aquapro Ultra-pure Water System (Chongqing, China). Unless other specified, all experiments were conducted at room temperature (RT).

2.2. Apparatus

Electrochemical experiments were performed with a CHI660C electrochemical workstation (Chenhua Co., Shanghai, China) controlled by a personal computer. A conventional three-electrode system was used in the measurements, with bare GCE (3 mm in diameter) or modified GCE as working electrode, a saturated calomel electrode (SCE) as reference electrode and a platinum wire as auxiliary electrode. All potentials given were referred to the SCE. Transmission electron microscope (TEM) images were obtained with a Tecnai G2–20 high-resolution TEM system (FEI, USA) opened at an accelerating voltage of 200 kV. Scanning electron microscopy (SEM) images were obtained by a Sirion 200 field emission SEM system (FEI, Holland). Ultrasonic cleaners (Branson2000, USA) and 320−S acidity meters (Mettler-Toledo, Switzerland) were used in this experiment.

2.3. Fabrication of the electrochemical biosensor

Prior to fabrication of biosensor, a bare GCE (diameter of 3 mm) was carefully polished with 0.05 μm Gamma alumina powder ($\gamma-Al_2O_3$) on chamois leather, and then washed ultrasonically in water and ethanol, respectively. An amount of 1 mg of graphene was dispersed in 1 mL of 10 mg mL^{-1} CTAB solution, and then the mixture was agitated in an ultrasonic bath for 1 h to get a black suspension. Then 5 μL of the homogeneous GR-CTAB solution (1 mg mL^{-1}) was cast onto the GCE and dried in air to yield the graphene modified electrode (GR/GCE). CS hydrogel was prepared by dissolving 5 mg CS in 1 mL acetic acid (0.1 M). Subsequently, 5 μL of the resulting CS-dispersed SA stock solution (1 mg mL^{-1}) was coated on the surface of the GR/GCE to yield the biosensor designated in the text as SA-CS/GR/GCE (Scheme 1). Other electrodes used were prepared with the similar procedure for comparison.

2.4. Analytical procedure

CEA solutions (25 μL) with different concentrations were mixed with 25 μL of prepared HRP-GNRs-HO conjugates (the preparation of GNRs and HO-GNRs-HRP conjugates were shown in the Supporting Information) to obtain the incubation solution. After incubation for 50 min at 37 °C, the as-prepared SA-CS/GR/GCE was immersed in the incubation solution and reacted for 20 min at 25 °C, followed by washing with washing buffer (10 mM PBS, pH=7.4, containing 3 mM SDS and 1% BSA). The electrochemical measurement was performed in 10 mM pH 7.0 PBS in the presence of 2 mM oPD. For the deoxygenated experiments, the electrolyte was bubbled with high-purity (99.99%) nitrogen for 15 min and nitrogen conditions were maintained during the experiment. After adding 5 μL of H_2O_2, differential pulse voltammetric (DPV) was recorded form −0.3 to −0.8 V at room

temperature with the parameters of increment potential, 0.004 V; pulse amplitude, 0.05 V; pulse width, 0.05 s; sample width, 0.0167; pulse period, 0.2 s; quiet time, 2 s. The measurement of clinical serum samples was performed with the same procedures mentioned above without any other treatments except 5-fold diluted using 10 mM pH 7.4 PBS.

3. Results and discussion

3.1. Characterization of GR and GNR

The obtained GR nanosheets were fully analyzed by TEM, XRD and Raman spectrum (Fig. S1 in the Supporting Information). TEM images of GR nanosheets showed a completely amorphous and disorder structure, clearly appearing semitransparent and flake-like shapes. In the XRD pattern, graphene has a characteristic peak centered at the Bragg angles of 22°, corresponding to the (002) plane of graphite crystal. In the Raman mapping image of GR, the typical *D* band was strong and located at 1335 cm^{-1}, which was usually assigned to sp^3-hybridized carbon. The *G* band around 1595 cm^{-1} arose from the E_{2g} phonon of sp^2-hybridized carbon (Wang et al., 2008). The high relative intensity D/G ratio (I_D/I_G) of GR was around 1.1, indicating the significant increase of number of the defective sites in graphite carbon and edge-plane-like defective sites appearance on the surface of GR (Zhou et al., 2009).

The synthesized GNRs were characterized by TEM and UV–vis spectra. As shown in Fig. S2A, the obtained GNRs with an average diameter of 14.3 ± 0.5 nm and a length of 52.5 ± 4.2 nm (corresponding to an aspect ratio of 3.7), were uniform in morphology and size. The typical absorption peak of GNRs appeared at 520 and 800 nm in the UV–vis spectrum (Fig. S2B), respectively, which was caused by the transverse and longitudinal surface plasmon resonance (Yasun et al., 2012).

3.2. Morphologic characterization of the fabricated biosensor

The SEM technique was performed for the morphologic characterization of the electrochemical biosensor. As shown in Fig. 1 (A), the GR displayed a thin crumpled paper-like structure with slightly scrolled edges, which was consistent with previous reports (Choucair et al., 2009; Wen et al., 2014). In Fig. 1(B), SA-CS films dispersed on the GC electrode surface exhibited a compact and gelatinous structure, which could be attributed to CS. Such a structure is favorable for the stability of the SA modified electrode. However, this compact film would have no benefits for SA effectively interacting with biotins and electron transfer. After introducing of GR into SA-CS films (Fig. 1(C)), the SA-CS/GR films become relatively uniform and loose, which present a composite structure of GR, CS and SA. This structure showed that these three aspects were linked up effectively in composite films, which could not only immobilize the SA stably and uniformly onto a glassy carbon surface, but also accelerate the electron transfer rate in the composite films. After electrodes modified with SA-CS/GR composite films incubation in the solution containing CEA and HO-GNRs-HRP conjugates, as shown in Fig. 1(D), SA-CS/GR composite films became more smooth, and appeared a lot of small white spots. From the inset for the high-resolution image, it can be seen

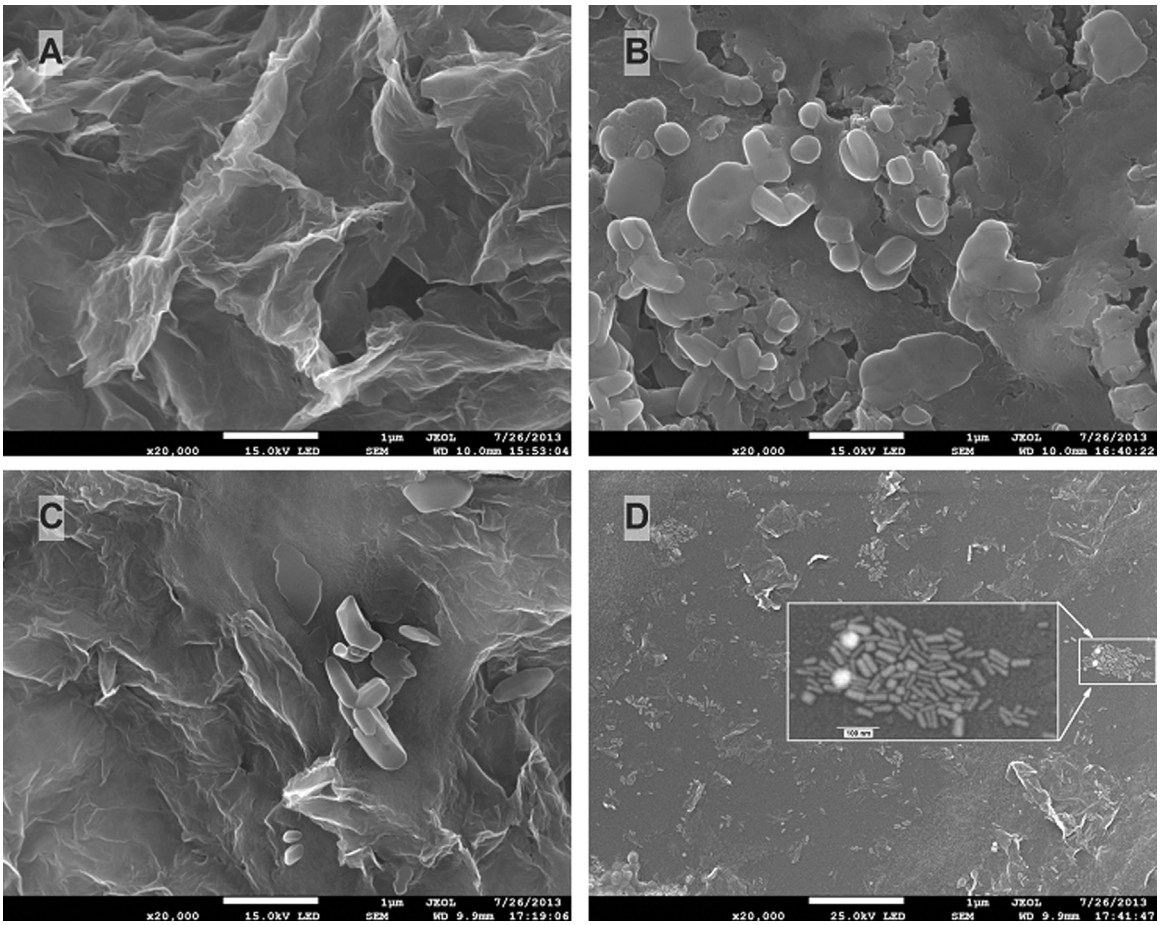

Fig. 1. SEM images of (A) GR/GCE, (B) SA-CS/GCE, (C) SA-CS/GR/GCE and (D) SA-CS/GR/GCE immersed in the incubation solution containing CEA and HO-GNRs-HRP conjugates. The inset is the high-resolution image.

that the white spots are the HO-GNRs-HRP conjugates immobilized in a well-dispersed way on the composite films.The result indicated HO-GNRs-HRP conjugates were captured successfully by the modified electrodes.

3.3. Electrochemical characterization of the fabricated biosensor

The chemical transformation and processes associated with the conductive electrodes surface of fabricated biosensors were measured by electrochemical impedance spectroscopy (EIS). Fig. S3A shows the Nyquist plots of EIS for different modified electrodes in 5 mM $[Fe(CN)_6]^{3-/4-}$ solution containing 0.1 M KCl. The frequency range was between 0.02 Hz and 10 kHz. At a bare GCE, the redox process of $[Fe(CN)_6]^{3-/4-}$ probe showed a much lower charge transfer resistance (R_{ct}) (curve a). The largest semicircle domain of the SA-CS/GCE was observed at high frequency area (curve b), which implies that there was the highest R_{ct} value to the redox probe at a GCE surface after SA-CS film modification, because both SA and CS was non-conductive materials. In contrast, when GR appeared in the composite film, the electron transfer resistance of the SA-CS/GR/GCE decreased very evidently (curve c), which implies that the unique properties of GR, such as an excellent electric conductivity, high electron transfer rate and abundant scrolled edge sites, could highly reduce the electron transfer resistance of the electrode surface and enhance the current response of the biosensor. After electrodes modified with SA-CS/GR composite films incubation in the solution containing CEA and HO-GNRs-HRP conjugates, the R_{ct} value of HO-GNRs-HRP/CEA/SA-CS/GR/GCE decreased further (curve d). Although introduce of CEA and HRP could increase R_{ct} value, when SA-CS/GR was first reacted with CEA and then treated with HO-GNRs-HRP conjugates, the whole R_{ct} decrease was observed due to the excellent electron-transport ability of gold nanorods. This correlates with the result observed from morphologic characterization in Fig. S2D.

To understand the use of GR for signal amplification, we compared the typical DPVs performances of the SA-CS/GR (Fig. S3B, curve c) film modified electrode with the SA-CS film modified electrode (Fig. S3B, curve b) treating with 5 ng mL^{-1} CEA. Under the same experimental conditions, a peak current response of 2.6 μA is obtained for SA-CS/GR/GCE, which is significantly higher than that of 0.7 μA for SA-CS/GCE. This illustrated that the introduction of GR into modified film greatly improves the sensitivity of biosensor, which might be attributed to the following reasons. First, high specific surface area of GR significantly increased the effective surface area of the electrode, which would immobilize more SA onto the surface of modified electrode. Second, excellent electrical conductivity and high electron transfer rate of GR could significantly promote the electrons transfer of electroactive species at the surface of electrodes. Third, the unique structure of scrolled edge sites at GR could effectively prevents the tendency towards SA aggregation on the surface of GCE, which provides a relatively loose structure for the composite film to react with biotinylated DNA probes. In the absence of CEA, a very low background DPV signal for SA-CS/GR/GCE is observed (Fig. S3B, curve a), which corresponded to reductive current of 2,2′-diaminobenzene, a trace of oxidized products caused by the direct oxidation of oPD slowly in the solution containing hydrogen peroxide (Lin et al., 2012).

3.4. Detection of CEA with the proposed biosensor

Under the optimized experimental conditions (as shown in the Supporting Information), the DPV currents were measured by varying the CEA concentration with the SA-CS/GR/GCE-based biosensor as shown in Fig. 2. The response peak current increased with the increase of different concentration of CEA analytes (Fig. 2 (A) from a to j), which indicates that the triple signal amplification was successfully implemented by using the HRP, GR and GNRs. Fig. 2(B) showed the calibration plot constructed by plotting the peak current against the logarithm of the CEA concentration. The SA-CS/GR/GCE-based biosensor exhibited a wide dynamic range between 5 pg mL^{-1} and 50 ng mL^{-1} with a correlation coefficient of 0.997 (n=9). The detection limit of CEA was 1.5 pg mL^{-1} (signal-to-noise ratio of 3). The observed dynamic range was much wider than the range between 0.1 ng mL^{-1} and 50 ng mL^{-1} of a fluorescent biosensor (Cui et al., 2008). The detection limit was also lower than those of carbon nanoparticle-enhanced electrochemical immunosensor (32 pg mL^{-1}) (Ho et al., 2009) and gold nanoparticles- enhanced electrochemical biosensor (500 pg mL^{-1}) (Shu et al., 2013).

To assess the selectivity of the biosensor, the DPV responses of the electrocatalytic reduction of DAP were measured for other common proteins such as myoglobin (Myo), Ferritin (Fer) and human immunoglobulin G (IgG). As shown in Fig. 3, it was found that 10-fold concentrations of Myo, Fer and IgG did not interfere with the CEA tests. The good selectivity of the biosensor is attributed to the high specificity and hairpin type configuration design of aptamer. The reproducibility and stability of the

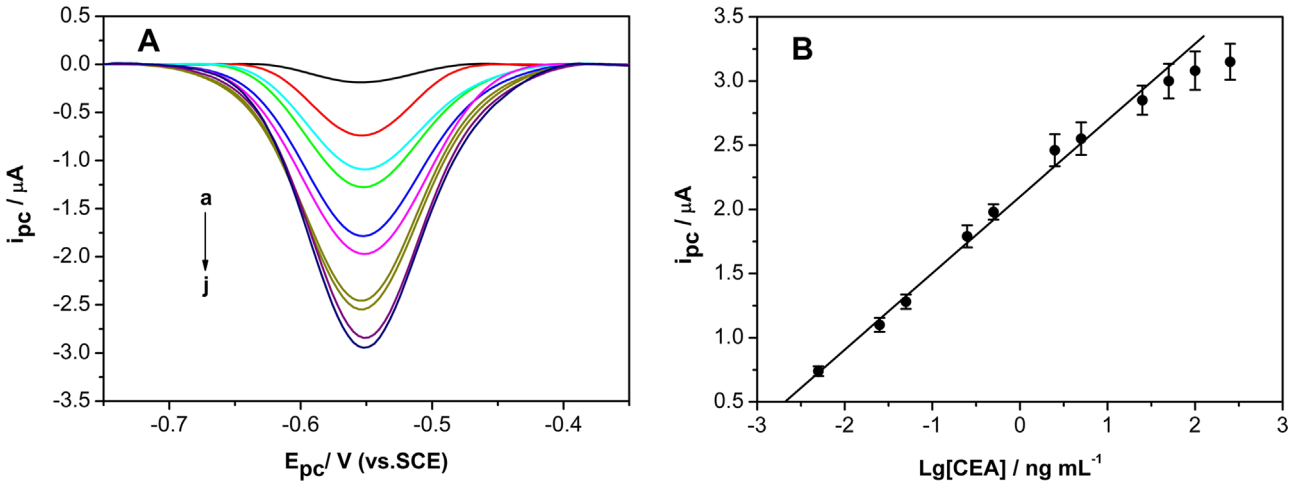

Fig. 2. (A) DPV responses of SA-CS/GR/GCE in determination buffer after incubated with different CEA concentrations (a–j): 0, 0.005, 0.025, 0.05, 0.25, 0.5, 2.5, 5, 25, 50 ng mL^{-1}. (B) Plot of the cathodal peak current for SA-CS/GR/GCE respect to the logarithm of the concentration of CEA (5 pg mL^{-1} to 50 ng mL^{-1}). Error bars were obtained from three experiments and the RSD was less than 5.2%.

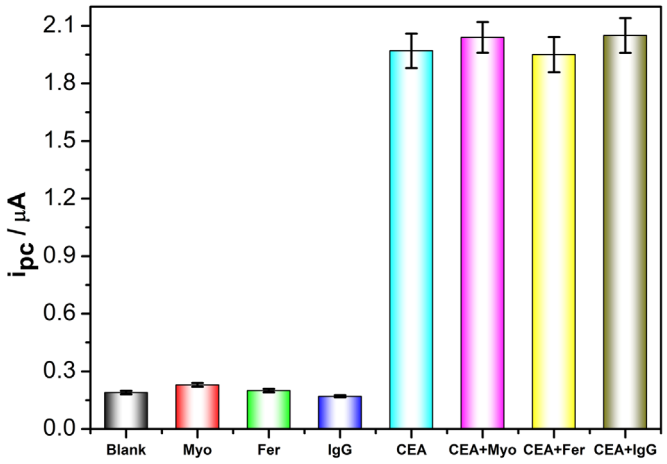

Fig. 3. Cathodal peak current response of the SA-CS/GR/GCE in determination buffer after incubated with (a) 0 ng mL^{-1} CEA, (b) 5 ng mL^{-1} Myo, (c) 5 ng mL^{-1} Fer, (d) 5 ng mL^{-1} IgG, (e) 0.5 ng mL^{-1} CEA, (f) e+5 ng mL^{-1} Myo, (g) e+5 ng mL^{-1} Fer, (h) e+5 ng mL^{-1} IgG. Error bars were obtained from three experiments.

biosensor were also investigated. Five electrodes, prepared under the same conditions independently, showed acceptable reproducibility with a RSD of 5.6% for the currents determined at a CEA concentration of 0.5 ng mL^{-1}. The interassay of the as-designed biosensor demonstrated the present biosensor could offer an acceptable reproducibility for detection of CEA. The storage stability of the biosensor was checked by measuring the DPV peak currents of SA-CS/GR/GCE in a determination buffer after incubated with 0.5 ng mL^{-1} CEA and HO-GNRs-HRP bioconjugate solution. The biosensor could maintain 92.7% of its initial response after being stored at 4 °C for 3 weeks, which indicated that the biosensor possessed good stability.

To demonstrate the potential of the proposed CEA biosensor in clinical application, 8 human serum samples from patients with lung diseases were measured by using SA-CS/GR/GCE-based biosensor and were compared to a chemiluminescence immunoassay. Table 1 shows the results, which presented that the estimated concentrations of CEA in these samples with as-prepared SA-CS/GR/GCE-based biosensor displayed a deviation ranging from −7.50% to 8.76% from those obtain with chemiluminescence. These results definitely illustrated that the SA-CS/GR/GCE biosensor was comparable to the clinical assay, exhibiting an acceptable accuracy. Most persons have detectable concentrations of circulating CEA. A CEA concentration of 5.0 ng mL^{-1} is commonly used cutoff point for distinguishing normal from abnormal level (Fletcher et al., 1986), which exactly fell in the dynamic range of the as-proposed SA-CS/GR/GCE-based biosensor, exhibiting great promise as a reliable technique for the detection of CEA in real biological samples.

Table 1
Comparison of the proposed method with chemiluminescence immunoassay for clinical CEA detection.

Clinical serum sample	Proposed method (ng mL^{-1})[a]	Chemiluminescence (ng mL^{-1})	Relative difference (%)
1	137.7 ± 5.37	130.8	5.28
2	11.1 ± 0.28	11.6	−4.31
3	130.3 ± 5.21	122.1	6.72
4	17.6 ± 0.49	17.1	2.92
5	0.91 ± 0.03	0.85	7.06
6	2.30 ± 0.09	2.22	3.60
7	1.48 ± 0.04	1.60	−7.50
8	1.49 ± 0.06	1.37	8.76

[a] Average of three measurements.

3.5. Generality of the platform for the detection of target DNA

To verify the wider applicability of the integrated sensing platform, we used the proposed biosensor to test target DNA. The principle of electrochemical detection for target DNA using HO-GNRs-HRP and SA-CS/GR/GCE is illustrated in Fig. S5. The target DNA (perfect-matched DNA) could strongly and selectively hybridize with the loop portion of the hairpin oligonucleotide on the gold nanorod surface to form a double-stranded structure and open the stem of the hairpin oligonucleotide. By analyzing the response peak current of DPV with the concentrations of target DNA, we obtained a linear relationship between the peak current value and the logarithm of the concentrations of target DNA over a range of 1.0 pM to 25 nM with a correlation coefficient of 0.997 (n=9, shown in Fig. 4(A)). The detection limit of target was 0.3 pM (signal-to-noise ratio of 3). To further test the specificity of our proposed approach, cathodal peak current responses of the biosensor versus perfectly complementary target DNA, one base-mismatched DNA and three base-matched DNA were shown in Fig. 4(B). It can be found that under the same experimental conditions, a peak current obtained for target DNA was significantly higher (more than 8.5 times) than that observed for one base-mismatched DNA at a DNA concentration of 0.5 nM. The high effective discrimination of the proposed biosensor enable us to differentiate the one base-mismatched DNA strands from the target DNA strands at very low concentration, which has great significance for the early detection of genetic point mutation, prevention and diagnostics of corresponding diseases.

4. Conclusions

In conclusion, we have developed a versatile, selective and sensitive amperometric biosensor by integrating the ultrahigh electrons transfer ability of GR, the classical avidin-biotin amplification system, and the specific aptamer-target recognition with the gold nanorods-based labeling technique. The alternative utilization of the oligonucleotide aptamers, rather than the antibodies for tumor marker CEA detection, paves a relatively cost-effective and novel way to electrochemical biosensors with a high specificity toward the targets. The triplex signal amplification was implemented for highly sensitive electrochemical detection of low-abundance proteins in biological fluids by introducing of graphene on biosensor surface to accelerate electron transfer, gold nanorods multilabeled with high molar ratio of HRP to HO and the classical avidin-biotin amplification system. More favorably, these results of target DNA detection made it abundantly clear that the proposed strategy can also be extended for detection of other relative biomarkers using different functional DNA structures, which shows great prospects in single-nucleotide polymorphisms analysis, biomedical sensing and application for accurate clinical diseases diagnostic.

Acknowledgments

Authors gratefully acknowledge support from the National Natural Science Foundation of China (Yuan-Di Zhao for Grant nos. 81271616, 81471697, Sheng-Fu Wang for 21175032, 21475032 and 21405035), the Key Technology R&D Program of Hubei Province (2014BBB003), Yellow Crane Talent (Science & Technology) Program of Wuhan City and Applied Basic Research Program of Wuhan City. We also thank Analytical and Testing Center (HUST) for the help of measurement.

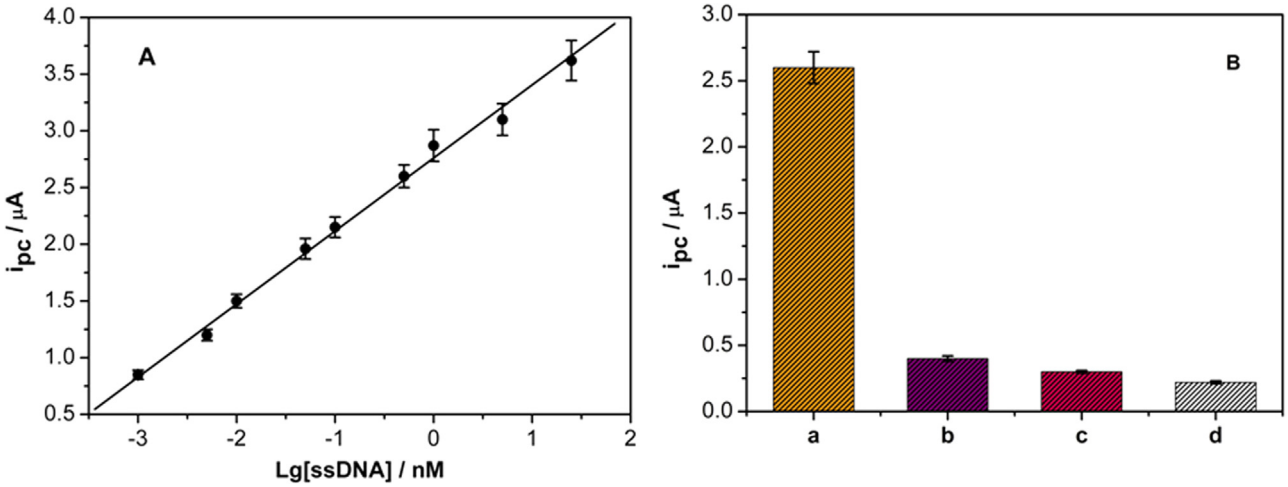

Fig. 4. (A) Plot of the cathodal peak current for SA-CS/GR/GCE with respect to the logarithm of the concentration of T-DNA (1.0 pM to 25 nM). Error bars were obtained from three experiments and the RSD was less than 4.6%. (B) Cathodal peak current response of the SA-CS/GR/GCE in determination buffer after incubated with (a) 0.5 nM T-DNA, (b) 0.5 nM one base-mismatched DNA, (c) 0.5 nM three base-mismatched DNA, (d) blank. Error bars were obtained from three experiments.

Appendix A. Supporting information

Supplementary data associated with this article can be found in the online version at http://dx.doi.org/10.1016/j.bios.2016.04.039.

References

Chen, H.J., Shao, L., Li, Q., Wang, J.F., 2013. Chem. Soc. Rev. 42, 2679–2724.
Chon, H., Lee, S., Son, S.W., Oh, C.H., Choo, J., 2009. Anal. Chem. 81 (8), 3029–3034.
Choucair, M., Thordarson, P., Stride, J.A., 2009. Nat. Nanotechnol. 4, 30–33.
Cui, R.J., Liu, C., Shen, J.M., Gao, D., Zhu, J.J., Chen, H.Y., 2008. Adv. Funct. Mater. 18, 2197–2204.
Deng, S.Y., Lei, J.P., Huang, Y., Cheng, Y., Ju, H.X., 2013. Anal. Chem. 85 (11), 5390–5396.
Fan, H., Xu, Y., Chang, Z., Xing, R., Wang, Q.J., He, P.G., Fang, Y.Z., 2011. Biosens. Bioelectron. 26, 2655–2659.
Fletcher, R.H., 1986. Ann. Intern. Med. 104, 66–73.
Ge, L., Wang, W., Hou, T., Li, F., 2016. Biosens. Bioelectron. 77, 220–226.
Hamilton, T.M., Dobie-Galuska, A.A., Wietstock, S.M.J., 1999. Chem. Educ. 76, 642–644.
He, Y., Wang, Z.G., Tang, H.W., Pang, D.W., 2011. Biosens. Bioelectron. 29, 76–81.
He, Y.Q., Zeng, K., Gurung, A.S., Baloda, M., Xu, H., Zhang, X.B., Liu, G.D., 2010. Anal. Chem. 82, 7169–7177.
Ho, J.A., Lin, Y.C., Wang, L.S., Hwang, K.C., Chou, P.T., 2009. Anal. Chem. 81, 1340–1346.
Huang, J., Yang, X.H., He, X.X., Wang, K.M., Liu, J.B., Shi, H., Wang, Q., Guo, Q.P., He, D. G., 2014. Trac. -Trend Anal. Chem. 53, 11–20.
Iliuk, A.B., Hu, L.H., Tao, W.A., 2011. Anal. Chem. 83, 4440–4452.
Kim, J.H., Morikis, D., Ozkan, M., 2004. Sens. Actuators B Chem. 102, 315–319.
Lao, Y.H., Phua, K.K.L., Leong, K.W., 2015. ACS Nano 9, 2235–2254.
Liang, K., Zhai, S.T., Zhang, Z.D., Fu, X.Y., Shao, J.W., Lin, Z.Y., Qiu, B., Chen, G.N., 2014. Analyst 139, 4330–4334.
Lin, Z.Y., Zhang, G.Y., Yang, W.Q., Qiu, B., Chen, G.N., 2012. Chem. Commun. 48, 9918–9920.
Liu, R., Liu, X., Tang, Y.R., Wu, L., Hou, X.D., Lv, Y., 2011. Anal. Chem. 83 (6), 2330–2336.
Pu, Y., Liu, Z.X., Lu, Y., Yuan, P., Liu, J., Yu, B., Wang, G.D., Yang, C.Y.J., Liu, H.X., Tan, W. H., 2015. Anal. Chem. 87, 1919–1924.
Shu, H.W., Wen, W., Xiong, H.Y., Zhang, X.H., Wang, S.F., 2013. Electrochem. Commun. 37, 15–19.
Springer, T., Bockova, M., Homola, J., 2013. Anal. Chem. 85, 5637–5640.
Tabar, G.R.H., Smith, C.L., 2010. World Appl. Sci. J. 8, 16–21.
Tang, L.H., Wang, Y., Li, J.H., 2015. Chem. Soc. Rev. 44, 6954–6980.
Wang, D., Li, Y., Lin, Z., Qiu, B., Guo, L., 2015. Anal. Chem. 87 (12), 5966–5972.
Wang, G.X., Yang, J., Park, J., Gou, X.L., Wang, B., Liu, H., Yao, J.J., 2008. Phys. Chem. C 112, 8192–8195.
Wang, K.M., Tang, Z.W., Yang, C.Y.J., Kim, Y.M., Fang, X.H., Li, W., Wu, Y.R., Medley, C. D., Cao, Z.H., Li, J., 2009. Angew. Chem. Int. Ed. 48, 856–870.
Wang, X.R., Hu, J.M., Zhang, G.Y., Liu, S.Y., 2014. J. Am. Chem. Soc. 136 (28), 9890–9893.
Wen, W., Bao, T., Yang, J., Zhang, M.Z., Chen, W., Xiong, H.Y., Zhang, X.H., Zhao, Y.D., Wang, S.F., 2014. Sens. Actuators B 191, 695–702.
Xu, Y.X., Shi, G.Q., Duan, X.F., 2015. Acc. Chem. Res. 48, 1666–1675.
Xue, S., Yi, H., Jing, P., Xu, W., 2015. RSC Adv. 5 (94), 77454–77459.
Yasun, E., Gulbakan, B., Ocsoy, I., Yuan, Q., Shukoor, M.I., Li, C.M., Tan, W.H., 2012. Anal. Chem. 84, 6008–6015.
Zhang, P., Zhuo, Y., Chang, Y., Yuan, R., Chai, Y.Q., 2015. Anal. Chem. 87 (20), 10385–10391.
Zhou, J., Lai, W.Q., Zhuang, J.Y., Tang, J., Tang, D.P., 2013. ACS Appl. Mater. Inter 5 (7), 2773–2781.
Zhou, M., Zhai, Y.M., Dong, S.J., 2009. Anal. Chem. 81, 5603–5613.
Zong, C., Wu, J., Wang, C., Ju, H.X., Yan, F., 2012. Anal. Chem. 84, 2410–2415.
Zuo, X.L., Xia, F., Xiao, Y., Plaxco, K.W., 2010. J. Am. Chem. Soc. 132, 1816–1818.